



Visible to Mid-infrared Waveband Photodetector Based on Insulator Capped Asymmetry Black Phosphorous

Qi Han¹, Yadong Jiang^{1,2}, Jiayue Han¹, Xiang Dong¹ and Jun Gou^{1,2*}

¹School of Optoelectronic Science and Engineering, University of Electronic Science and Technology of China, Chengdu, China,

²State Key Laboratory of Electronic Thin Films and Integrated Devices, University of Electronic Science and Technology of China, Chengdu, China

OPEN ACCESS

Edited by:

Jinshui Miao,
Shanghai Institute of Technical
Physics (CAS), China

Reviewed by:

Shaojuan Li,
Changchun Institute of Optics, Fine
Mechanics and Physics (CAS), China
Zaixing Yang,
Shandong University, China

*Correspondence:

Jun Gou
goujun@uestc.edu.cn

Specialty section:

This article was submitted to
Optics and Photonics,
a section of the journal
Frontiers in Physics

Received: 15 May 2021

Accepted: 09 August 2021

Published: 16 September 2021

Citation:

Han Q, Jiang Y, Han J, Dong X and
Gou J (2021) Visible to Mid-infrared
Waveband Photodetector Based on
Insulator Capped Asymmetry
Black Phosphorous.
Front. Phys. 9:710150.
doi: 10.3389/fphy.2021.710150

Processing layer-dependent direct band gap and good absorption coefficient especially in the mid-infrared band, black phosphorous is believed to make a contribution superior to that of graphene in broadband photodetectors. The narrow band gap of 0.3 eV for bulk black phosphorous helps to absorb infrared radiation while a relatively large dark current under zero gate voltage is inevitable. Few layer black phosphorous sheets with asymmetrical thickness sealed in an insulator for protection is designed and explored for photosensitive mechanism in this work. Saturable absorption dominates the light harvesting process in visible light detection and thus limits maximum photocurrent to 3.3 and 1.4 μA for 520 and 650 nm lasers with a dark current of 0.7 μA . While in near-infrared wavelength, a responsivity of 0.12 A/W is induced for 808 nm free of adsorption saturation even if the incident power is increased to 200 mW/cm^2 . Discrimination for the origin of the photo-response in short wavelength is conducted and the abnormal negative and nearly constant photocurrent in mid-infrared, irrelevant to inhomogeneous thickness, reveals the photothermal effect in a black phosphorous sheet. This work unravels various photoelectric features in black phosphorous and paves the way to designing more outstanding broadband photodetectors based on black phosphorous.

Keywords: black phosphorous, mid-infrared, broadband, saturable absorption, homogeneous junction

INTRODUCTION

Black phosphorous (BP) is a two-dimensional material with a layer-dependent bandgap. Although the orthorhombic crystal group as well as some basic parameters such as lattice dimensions have been determined by Brown et al. in 1965 [1], detailed research of BP boomed after the successful exfoliation of graphene [2]. A poor absorption coefficient gets graphene over a barrel in optical detection [3]. Thus, a series of two-dimensional material including BP is investigated and made instead. The bandgap of BP monotonically decreases from 1.8 to 0.3 eV as the number of layers grows [4]. Zhang et al. confirmed the layer-dependent feature of phosphorene through photoluminescence for two to five layers BP [5]. In bulk form, BP processes a direct bandgap of 0.3 eV, especially suitable for mid-infrared light detection. Several previous works present BP's infrared light harvesting effect, the wavelength ranging from 1.5 to 7.7 μm [6–10]. A silicon-compatible photovoltaic BP photodetector is made by Youngblood et al. and demonstrates fast response and low dark current [6]. Deng constructs a van der Waals heterojunction of black phosphorous and MoS_2

with a high on-off ratio and reasonable responsivity in the visible wavelength [11]. Zheng further enhanced the photocurrent of BP – MoS₂ heterojunction by 10³ with the help of surface acoustic waves [12]. Although the chemical synthesis of BP is eligible under restricted conditions [13], there is still difficulty in massive application for optical-electronic devices of BP due to the degradation in an ambient environment, which is accelerated by water explosion and laser illumination [14]. To overcome this obstacle, Liu et al. encapsulated BP in a graphene layer and got high responsivity and an air-stable photodetector [15]. Ren synthesized BP nanosheets by a liquid exfoliation method and demonstrated environmental robustness under irradiation [16]. Illarionov et al. concealed a BP transistor in Al₂O₃, and the fundamental characteristics keep for at least 8 mo [17]. Although the basic electric feature, photo-sensitive character, as well as the protection method are investigated for BP, the research remains in a uniform and homogeneous condition.

In this work, asymmetric BP is fabricated and serves as a photodetector. Saturable absorption effect is observed in the visible waveband. That is, the amplitude of the photocurrent fails to grow if the incident radiation power is increased to a certain plateau. Besides, these plateaus diverge for different wavelengths. The pinning effect shaped the IV curve of asymmetric BP. An uneven quasi Fermi level accounts for the observed apparent and fast response in visible and near-infrared waveband. A modeling of a BP sheet by use of technology computer aided design (TCAD) shows distinct line shapes of symmetric and asymmetric conditions, confirming the theory of uneven p doping of asymmetric BP. Moderate responsivity (several hundred milli-amperes per watt) and relatively fast response (~200 μs) is acquired for visible light. More details of the energy band as well as bias dependent photocurrent can be provided by simulation. Then, the photo-response in the mid-infrared band is measured. The response is believed to originate in the heat transition process, observed from a negative photocurrent independent of sheet uniformity. The photosensitive mechanism for mid-infrared is contrary to visible and near-infrared waveband. Compared to an ordinary BP sheet, the asymmetric BP demonstrates higher responsivity and wider waveband sensitivity.

MATERIALS AND METHODS

Au electrodes are deposited on 300 nm SiO₂/Si substrate with a 10-nm chromium moist layer, followed by BP transferring by use of the universal two-dimensional material dry transfer method [18, 19]. Electric features measurement is carried on bare BP. The BP bulk material is purchased from Nanjing MuKe Nanotechnology Co., Ltd. Then, a layer of exfoliated h-BN, purchased from Six-Carbon Technology (Shenzhen, China), is also transferred, covering the BP. The photocurrent is collected by a PDA source meter. A narrow band filter centered at 3.5 or 4.5 μm with a full width at half maximum of 500 nm is placed before a black body for certain mid-infrared wavelengths. The spot size for these mid-infrared filtered lights is estimated as 2 cm². In addition, the time-resolved response is recorded with a manual chopper, so the response speed recorded is slower than the reality.

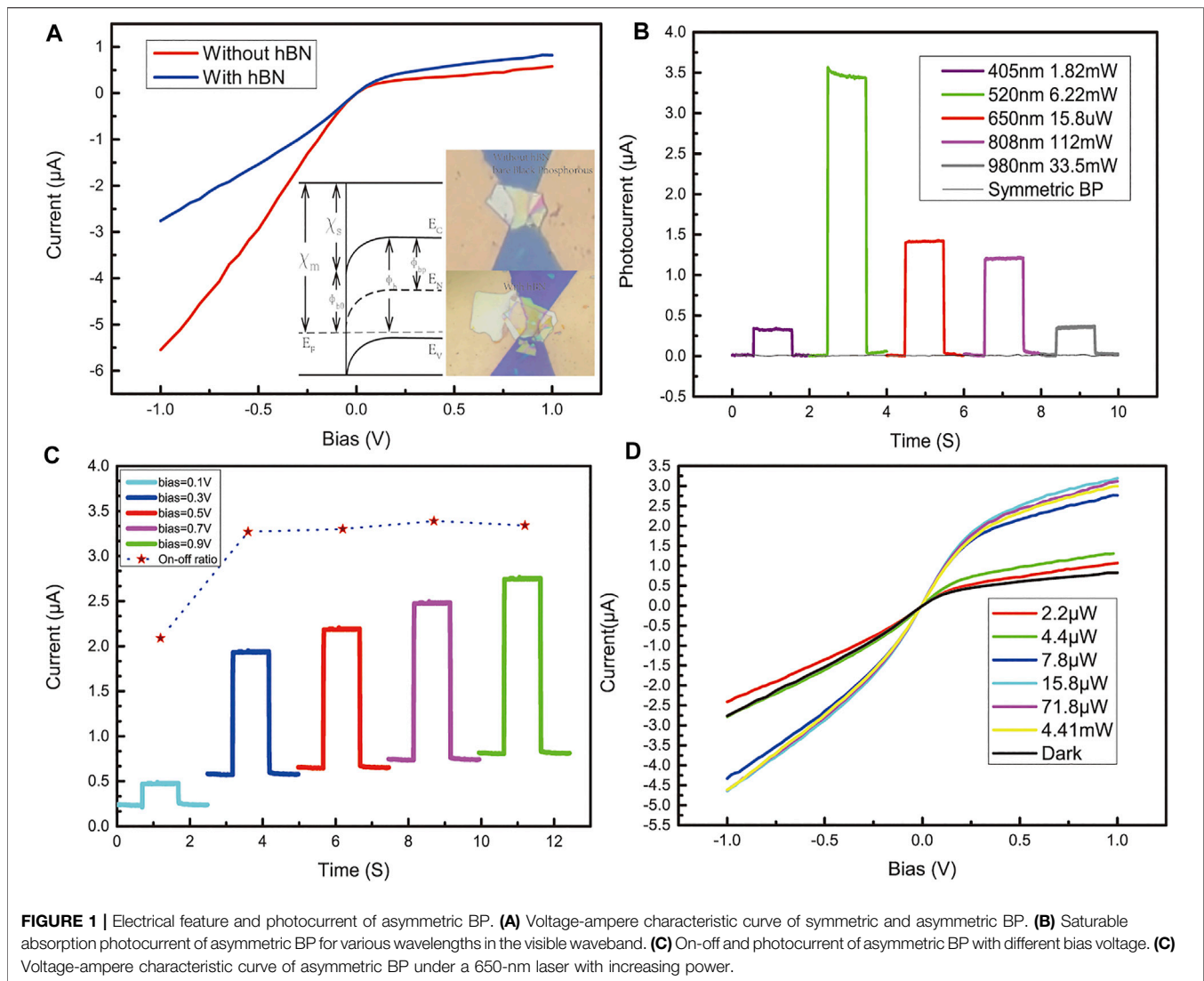
RESULTS AND DISCUSSION

A pair of obtuse angle gold electrodes is prepared by lithography and patterning of electrodes, and then an asymmetric, bare BP sheet is transferred on an SiO₂/Si substrate, as illustrated in **Figure 1A**. Uneven thickness is clearly observed from the different color in the upper part of the inset. As previous research shows, thickness of the BP varies with the color under an optical microscope and shows weak periodic feature. This holds for both epitaxial of high-crystalline and exfoliated BP condition [13, 20]. To apply the method to asymmetric BP, various types of setups of BP and metal electrodes are evaluated by profilometer and metallographic microscope; see supplement information.

A typical Schottky barrier in a junction of metal and BP is $\phi_{b0} = \chi_m - \chi_s$, where χ_m and χ_s are work function of the metal and ionization potential of BP. Conduction and valance band bend according to the barrier. For our device, the energy band edges bend near the interface due to a transition of electron from a metal electrode to BP. The presence of a barrier together with Fermi-Dirac distribution shapes the IV curve. A typical IV curve of a BP sheet is shown in **Figure 2D**. A schematic diagram and symbols are shown in the inset of **Figure 1A**. If the work function of the metal is very close to the ionization potential of the semiconductor, ϕ_{b0} is little and an ohmic contact is expected. In this condition, the IV curve is a straight line.

For our asymmetric BP, the situation is different. The IV curve shows an abrupt change of slope around zero bias in **Figure 1A**. Curvature tends to be gigantic in both the positive and negative bias voltage range. Besides, the rectifying ratio reaches 9.2, see IV curve without hexagonal boron nitride (h-BN). It is the red line in **Figure 1A** for bare BP. This behavior of the IV curve is different from ohm-contact BP field-effect transistors [21], a heterojunction formed by BP and another semiconductor [22, 23] or a Schottky connection formed from a connection of a semiconductor and metal.

To explain this unique electric, a dipole formed by pinning effect is introduced. At the interface of metal and semiconductor contact, there is an always finite density of states called metal-induced gap states (MIGS) with complex wave vector. The abrupt change of geometry results in an energy level splitting at the interface. As a result, the metal allows states at all energies [24]. Sometimes its influence cannot be ignored. These metal-induced gap states give a dipole $D = \alpha(E_F - E_N) = \alpha(\phi_{bp} - \phi_b)$ at the interface. E_N here is the neutrality level, i.e., the Fermi-level E_F at which the dipole would be zero. The α here represents pinning strength and $\phi_{bp} = E_C - E_N$ is the barrier height in the limit of strong pinning. The dipole then changes the barrier in turn. When we don't care about capacity of the junction in our low frequency situation, the pinning phenomena abstractly represented by the dipole can be simplified to a resistance near the interface. Its sign depends on the relative position of energy bands. The influence of the dipole gradually attenuates as the focus goes into the semiconductor. With a lager gap between E_F and E_N , a heavily p doped BP part is influenced more by this effect; thus, the p doping is relived.

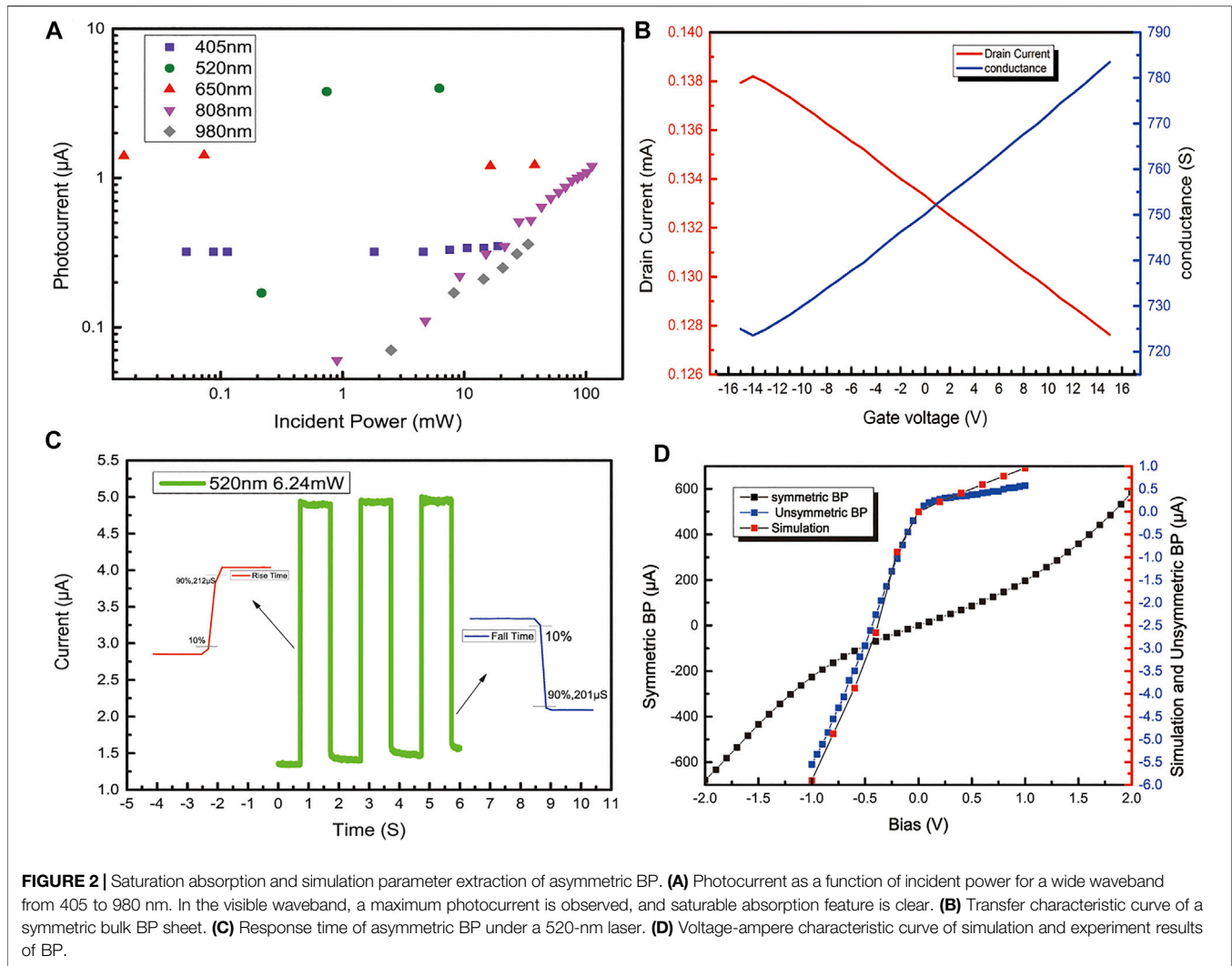


When we take a closer look at the IV curve of asymmetric BP, there is a combination of ohmic contact and Schottky contact. In a very little range of bias voltage around zero, there is still a curvature in the IV curve, meaning an inevitable barrier is present. In the process of forming the ohmic contact, electrons in metal can move fluently in BP and thus deduce BP's original p doping and uplift the quasi Fermi level for holes. Finally, more metal-induced gap states are occupied, and the intrinsic doping is decreased. As a result, a more balanced IV curve is observed.

BP lacks water, oxygen, and light stability [14]. The existing strategy to make better stability includes covalent functionalization [25] and additional material capping [15]. In this work, to decrease the degradation of BP, a layer of h-BN is exfoliated and transferred onto the BP, as shown in the bottom part of the inset of **Figure 1A**. The line shape of volt-ampere characteristics stays the same, while the amount of slope rate unignorablely decreases. The rectifying ratio declines to 3.2, implying the barrier of the junction is attenuated by the h-BN capping. In the pinning diagram, the dipole as well as the pinning

strength relies on the gap in the junction. The gap is varied in the process of h-BN transferred due to additional force and weight and it may be the reason of the change in IV curve after the transferring of the h-BN. In the process of preparing the device, to liberate the sample from PDMS to the substrate, the holder for the sample should be heated. BP requires less than 40°C to be released, and h-BN usually requires 75°C. The press and the heat may strengthen the connection of BP and the metal. The influence of dielectric layers to the doping type and level is also reported by Nathan et al. [6], but it is not applicable in the asymmetric BP here, for the absolute value changes in different ways for positive and negative bias. Although encapsulated, the device may be degraded 1 mo later, and the speed of degradation can be accelerated by illumination to our experience.

Due to this asymmetric characteristic, optical electronic performance is also enhanced for visible and near-infrared wavelengths. Compared to a uniform BP sheet, an asymmetric device provides larger photocurrent in visible and near-infrared wavelength, as shown in **Figure 1B**. Little photocurrent can be



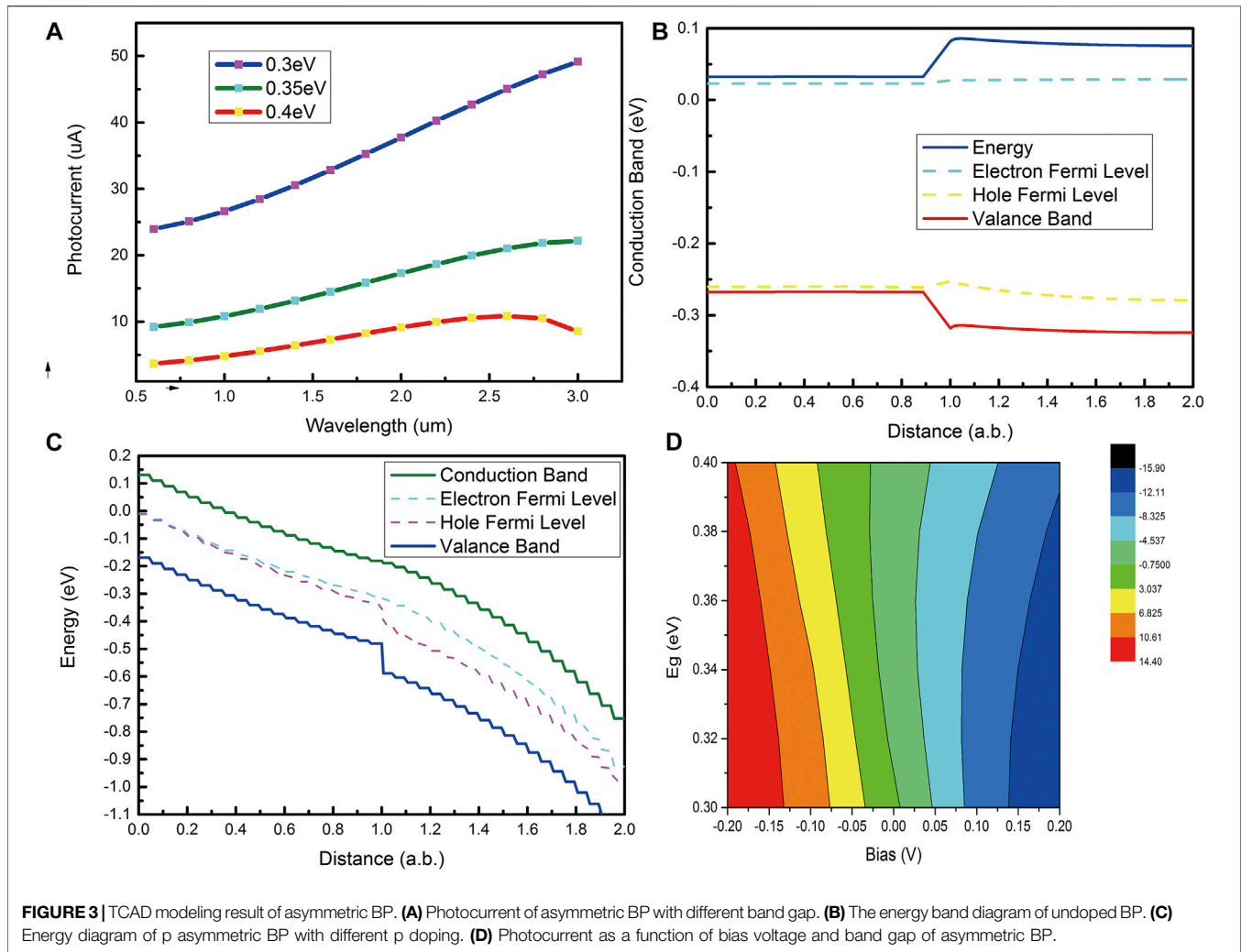
acquired for an ordinary symmetric BP. The optical sensitive feature is distinct from many traditional materials, such as silicon due to its small and direct band gap (~ 0.3 eV). For a photon with energy much larger than the band gap but not enough to induce an Auger effect, there is still only one pair of photo-excited carriers. Excess energy is turned into kinetic energy of electrons and phonons. Therefore, when a photodetector made of BP works at the visible waveband, photo energy leakage is inevitable. As a result, the absorption coefficient of bulk BP to photons between 0.3 and 3 eV is relatively poor [26]. The saturable absorption phenomena is also recorded for BP quantum dots for ultrafast photonics [27]. In **Figure 1B**, the least energy eligible for saturable absorption is applied on the asymmetric BP and corresponding photocurrent is plotted. No monotonous law is found in the relationship between max photocurrent and least saturable absorption energy. However, larger energy can be more acceptable for longer wavelengths. The measurement is limited by max power the lasers can provide in the 808 and 980 nm cases.

Gate voltage is usually needed for ordinary BP photodetectors to achieve reasonable on-off ratio. Varying the gate voltage

frequently in analog devices may require additional preparing time and accuracy in practical application. In this experiment, the gate voltage is invariant. As illustrated by **Figure 1C**, asymmetric BP can reach an on-off ratio from 2.05 to 3.3 with the bias ranging from 0.1 to 0.9 V. The photo current grows proportionately with dark current when the bias is higher than 0.3 V. The photocurrent bias dependency reminds us that saturable photocurrent can be enhanced by a stronger directional electric field.

The saturation of photocurrent can be as soon as the power of incident light is increased; see **Figure 1D** for details of a 650 nm case. The overall current reaches $3.04 \mu\text{A}$ under an incident power of $15.8 \mu\text{W}$. In addition, the current slightly decreases when a higher laser power of $71.8 \mu\text{W}$ or 4.41 mW is applied. The photocurrent is opposite for a low power of $2.2 \mu\text{W}$. This is counterintuitive. The incident light may set the device in a small signal mode. The dipole induced by the pinning effect changes its sign for reversed bias.

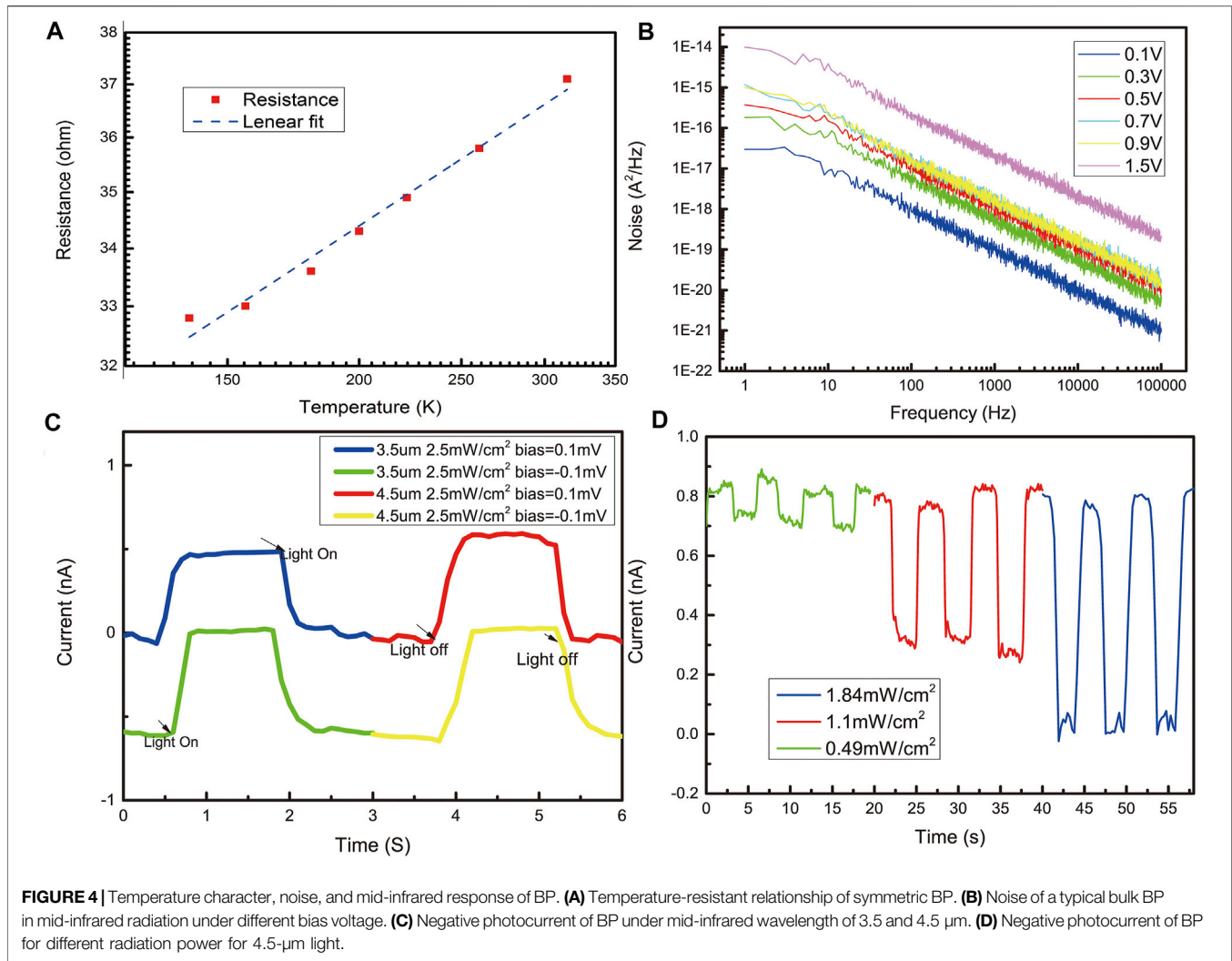
A comprehensive relationship of photocurrent and incident power is shown in **Figure 2A**. The sequence of wavelength of minimum cut off saturation power is $15.8 \mu\text{W}$, 1.82 , and



6.22 mW for 650, 405, and 520 nm. Among these, the minimum saturable energy of 405 and 650 nm is limited by the least power the laser can provide. The slope of linear fit of the photocurrent and incident power is zero if the device works at the saturable state. The responsivity is evaluated as 0.12 $\mu\text{A}/\text{W}$ for an 808-nm laser. The responsivity of the device is inferior to typical commercial photodetectors, but there is a large improvement to a symmetric BP sheet. Apart from responsivity, another important parameter of photodetectors is its speed. The rising and falling time of the device is relatively short for 212 and 201 μs , respectively, see **Figure 2C**. The fast rehabilitation of the photo response indicates enough shallow energy traps in the BP sheet, according to the theory of the Hornbeck–Haynes model [10, 28].

To analyze the carriers and verify our model, especially the dipole introduced by pinning effect, a simulation by means of TCAD is conducted. The transfer characteristic curve of a symmetric BP sheet is measured. The result is in **Figure 2B**. Hole mobility of BP is extracted following $\mu = L/(WC_{ox}V_{ds}) \times \partial I_{ds}/\partial V_{ds}$, where L, W refers to the length and width of the channel, C_{ox} denotes oxide capacitance per

unit area, V_{ds} is the bias voltage, and $\partial I_{ds}/\partial V_{ds}$ refers to the differential conductance. The value of hole mobility is $321\text{cm}^2/(\text{V}\cdot\text{s})$, and electron mobility adopts $46\text{cm}^2/(\text{V}\cdot\text{s})$, following the relationship of the proportional ratio mentioned in [9, 29]. The doping of BP is critical in the setup of the simulation. A homogenous junction is modeled by denoting different intrinsic p doping in two halves of the BP, just the same as discussed previously. The difference of p doping between two parts is $2.8 \times 10^{14}\text{cm}^{-3}$ in concentration, representing the dipole of the pinning effect. The simulation is in good accordance with the experiment, as shown in **Figure 2D**. There is multiplicity in the solving of the passion equation if a certain result is required. The effective mass density of states and the mobility determine the absolute value of static current, but the relative ratio of the forward current to the backward current and the line shape of the voltage-ampere reflects the essence of our asymmetric BP, which is of interest. The thickness of a nanosheet also influences the bandgap of the BP, so a slight change is also applied to the band gap parameter of a two-end in the model. Asymmetric BP shares a two-segment approximate linear voltage-ampere characteristic curve. And for symmetric



BP, an IV curve of standard heterojunction is acquired in good agreement with measuring result as well.

Further information can be deduced from the simulation result, and it is helpful in the analysis of mid-infrared photo-response of BP. A dependency of photocurrent on wavelength for different band gaps is present in **Figure 3A**. The model for optical response is complicated and the photocurrent relies on incident power, which is set in the simulation, so the absolute value of the photocurrent is not eligible. However, relative strength of photon absorption coefficient and peak of sensitive waveband are worth noting. The band diagram of non-doped, zero biased and doped on two parts, respectively, biased BP sheets are respectively illustrated in **Figures 3B,C**. The carrier density can be deduced from the distance between quasi Fermi level with its conduction or valance band. There is an abrupt change of density of holes at the interface of the homogenous junction in **Figure 3C**. The holes accumulate more on the less doped part and a sudden decrease appears on the heavily doped part. This is intuitive due to the holes' diffusion effect. Dependency of photocurrent on the bias voltage and band gap of BP is shown in **Figure 3D**. This

simulation helps find an open circuit voltage and discover photo-sensitive characters of new combination sets of asymmetric BP devices.

Asymmetric BP is superior in visible and near-infrared waveband. However, in mid-infrared wavelength, a photothermic effect dominates the photocurrent. So, there is no apparent difference between asymmetric and symmetric BP in mid-infrared detection. The relationship of resistance and temperature of a symmetric BP sheet is shown in **Figure 4A**. As temperature increases, the resistance of BP also increases; thus, a positive temperature-resistant coefficient is observed.

A table of photodetectors associated with BP is summarized in **Table 1**. All the mid-infrared BP listed used a lock-in amplifier. Employing a lock-in method can filter the noise largely, so the signal to noise is greatly enhanced. A preamplifier is a recurring option combined with a lock-in amplifier. With the help of a lock-in amplifier and preamplifier, the responsivity can be enhanced. However, it is not the nature of the device. Although our device requires low bias, a time-resolved photocurrent can be observed.

TABLE 1 | A summary of black phosphorous photodetectors.

Material	Wavelength	Responsivity	Measurement method	Response time (frequency)	Ref
BPs/silicon	Near-infrared telecom band	657 mA/W	Lock-in amplifier	~200 ps	[6]
BP nanosheets	365–546 nm	2.2 μ A/W	Source meter	Several seconds	[16]
BPs	2 μ m	10 ⁴ A/W	Parameter analyzer	3 db bandwidth: 156 kHz	[7]
BPs	3, 4, 5, 7.7 μ m	8 mA/W	Lock-in amplifier	1.3 GHz	[9]
			77 K		
BPs	830 nm	53 A/W	Source meter	Hundreds of milliseconds	[31]
BPs	532 nm to 3.39 μ m	82 A/W	Lock-in amplifier	Several kHz	[10]
Graphene/BP	1550 nm	3.3 \times 10 ³ A/W	Source meter	4 ms	[15]
BPs	Visible to 980 nm, 3.5 μ m, 4.5 μ m	0.12 A/W	Source meter	~200 μ s (visible)	This work

The photocurrent is negative and little in absolute value, as shown in **Figure 4C** for 3.5 and 4.5 μ m incident power. Negative temperature-resistance coefficient of BP may account for this abnormal effect [30], though positive temperature-resistance coefficient is also reported [20]. The incident light serves as a heater and the BP sheet presents its metallicity. A dark current of ~0.5 nA is set for the BP and the photocurrent is approximately equal in value but opposite in direction, as shown in **Figure 4C**. The responsivity is evaluated as 0.9 mA/W and noise equivalent power is $1.42 \times 10^{-9} \text{ WHz}^{-1/2}$. As a result, a total current falls around zero. We restrict bias to 0.1 V to decrease shot noise, as the shot noise can vary in order of magnitude with bias. In fact, time-resolved photocurrent cannot be extracted if a large dark current is present for both symmetric and asymmetric BP sheets. In **Figure 4D**, the relationship of mid-infrared photocurrent and the incident power for 4.5- μ m light is shown. The photocurrent is negative. As the incident power is increased, it takes longer to reach the maximum photocurrent. The total current is saturable to around zero, and a thorough mechanism requires more exploration.

CONCLUSION

Asymmetric BP is superior in photodetection to ordinary BP in visible and near-infrared. The saturable absorption effect discovered restricts the BP's pure photodetection practical application. However, it is still optimistic to further investigate and design certain optical devices by optimizing the parameters of asymmetric BP for its promising on-off ratio and relatively fast speed. Simulation is confirmed with the experiment in the electric feature and provides insight to developing novel appliances for BP. The temperature resistance coefficient may clarify BP's abnormal opposite photocurrent in the mid-infrared

REFERENCES

1. Brown A, and Rundqvist S. Refinement of the Crystal Structure of Black Phosphorus. *Acta Cryst* (1965) 19:684–5. doi:10.1107/S0365110X65004140
2. Novoselov KS, Geim AK, Morozov SV, Jiang D, Zhang Y, Dubonos SV, et al. Electric Field Effect in Atomically Thin Carbon Films. *Science* (2004) 306: 666–9. doi:10.1126/science.1102896

waveband. All these experiments and analyses can pave the way for designing more outstanding broadband photodetectors based on BP.

DATA AVAILABILITY STATEMENT

The original contributions presented in the study are included in the article/**Supplementary Material**, further inquiries can be directed to the corresponding authors.

AUTHOR CONTRIBUTIONS

JG conceived and supervised the project. QH prepared the device and performed the photocurrent measurements and characterizations. XD and YJ set up the experimental platform, YJ and XD performed the data analysis. QH wrote this paper. All authors discussed the results and commented on the manuscript.

FUNDING

This work is supported by the National Natural Science Foundation of China (Grant No. 61875031) and National Natural Science Foundation-Outstanding Youth Foundation (No. 61922022).

SUPPLEMENTARY MATERIAL

The Supplementary Material for this article can be found online at: <https://www.frontiersin.org/articles/10.3389/fphy.2021.710150/full#supplementary-material>

3. Blake P, Hill EW, Castro Neto AH, Novoselov KS, Jiang D, Yang R, et al. Making Graphene Visible. *Appl Phys Lett* (2007) 91:063124. doi:10.1063/1.2768624
4. Carvalho A, Wang M, Zhu X, Rodin AS, Su H, and Castro Neto AH. Phosphorene: From Theory to Applications. *Nat Rev Mater* (2016) 1:16061. doi:10.1038/natrevmats.2016.61
5. Zhang S, Yang J, Xu R, Wang F, Li W, Ghufuran M, et al. Extraordinary Photoluminescence and Strong Temperature/Angle-Dependent Raman

- Responses in Few-Layer Phosphorene. *ACS Nano* (2014) 8:9590–6. doi:10.1021/nn503893j
6. Youngblood N, Chen C, Koester SJ, and Li M. Waveguide-integrated Black Phosphorus Photodetector with High Responsivity and Low Dark Current. *Nat Photon* (2015) 9:247–52. doi:10.1038/nphoton.2015.23
 7. Huang L, Tan WC, Wang L, Dong B, Lee C, and Ang K-W. Infrared Black Phosphorus Phototransistor with Tunable Responsivity and Low Noise Equivalent Power. *ACS Appl Mater Inter* (2017) 9:36130–6. doi:10.1021/acsmi.7b09713
 8. Ye L, Li H, Chen Z, and Xu J. Near-Infrared Photodetector Based on MoS₂/Black Phosphorus Heterojunction. *ACS Photon* (2016) 3:692–9. doi:10.1021/acsp Photonics.6b00079
 9. Chen X, Lu X, Deng B, Sinai O, Shao Y, Li C, et al. Widely Tunable Black Phosphorus Mid-infrared Photodetector. *Nat Commun* (2017) 8:1672. doi:10.1038/s41467-017-01978-3
 10. Guo Q, Pospischil A, Bhuiyan M, Jiang H, Tian H, Farmer D, et al. Black Phosphorus Mid-infrared Photodetectors with High Gain. *Nano Lett* (2016) 16:4648–55. doi:10.1021/acs.nanolett.6b01977
 11. Deng Y, Luo Z, Conrad NJ, Liu H, Gong Y, Najmaei S, et al. Black Phosphorus-Monolayer MoS₂ van der Waals Heterojunction p-n Diode. *ACS Nano* (2014) 8:8292–9. doi:10.1021/nn5027388
 12. Zheng S, Wu E, Feng Z, Zhang R, Xie Y, Yu Y, et al. Acoustically Enhanced Photodetection by a Black Phosphorus-MoS₂ van der Waals Heterojunction p-n Diode. *Nanoscale* (2018) 10:10148–53. doi:10.1039/c8nr02022a
 13. Xu Y, Shi X, Zhang Y, Zhang H, Zhang Q, Huang Z, et al. Epitaxial Nucleation and Lateral Growth of High-Crystalline Black Phosphorus on Silicon. *Nat Commun* (2020) 11:1330. doi:10.1038/s41467-020-14902-z
 14. Huang Y, Qiao J, He K, Bliznakov S, Sutter E, Chen X, et al. Interaction of Black Phosphorus with Oxygen and Water. *Chem Mater* (2016) 28:8330–9. doi:10.1021/acs.chemmater.6b03592
 15. Liu Y, Shivnanju BN, Wang Y, Zhang Y, Yu W, Xiao S, et al. Highly Efficient and Air-Stable Infrared Photodetector Based on 2D Layered Graphene-Black Phosphorus Heterostructure. *ACS Appl Mater Inter* (2017) 9:36137–45. doi:10.1021/acsmi.7b09889
 16. Ren X, Li Z, Huang Z, Sang D, Qiao H, Qi X, et al. Environmentally Robust Black Phosphorus Nanosheets in Solution: Application for Self-Powered Photodetector. *Adv Funct Mater* (2017) 27:1606834. doi:10.1002/adfm.201606834
 17. Illarionov YY, Waltl M, Rzepa G, Kim J-S, Kim S, Dodabalapur A, et al. Long-Term Stability and Reliability of Black Phosphorus Field-Effect Transistors. *ACS Nano* (2016) 10:9543–9. doi:10.1021/acsnano.6b04814
 18. Huang Z, Jiang Y, Han Q, Yang M, Han J, Wang F, et al. High Responsivity and Fast UV-Vis-Short-Wavelength IR Photodetector Based on Cd₃As₂/MoS₂ Heterojunction. *Nanotechnology* (2019) 31:064001. doi:10.1088/1361-6528/ab51d3
 19. Buscema M, Barkelid M, Zwiller V, van der Zant HSJ, Steele GA, and Castellanos-Gomez A. Large and Tunable Photothermoelectric Effect in Single-Layer MoS₂. *Nano Lett* (2013) 13:358–63. doi:10.1021/nl303321g
 20. Castellanos-Gomez A, Vicarelli L, Prada E, Island JO, Narasimha-Acharya KL, Blanter SI, et al. Isolation and Characterization of Few-Layer Black Phosphorus. *2D Mater* (2014) 1(2):025001. doi:10.1088/2053-1583/1/2/025001
 21. Li L, Yu Y, Ye GJ, Ge Q, Ou X, Wu H, et al. Black Phosphorus Field-Effect Transistors. *Nat Nanotech* (2014) 9:372–7. doi:10.1038/nnano.2014.35
 22. Gehring P, Urcuyo R, Duong DL, Burghard M, and Kern K. Thin-layer Black phosphorus/GaAs Heterojunction P-N Diodes. *Appl Phys Lett* (2015) 106:233110. doi:10.1063/1.4922531
 23. Chen P, Xiang J, Yu H, Zhang J, Xie G, Wu S, et al. Gate Tunable MoS₂-black Phosphorus Heterojunction Devices. *2D Mater* (2015) 2:034009. doi:10.1088/2053-1583/2/3/034009
 24. Léonard F, and Tersoff J. Role of Fermi-Level Pinning in Nanotube Schottky Diodes. *Phys Rev Lett* (2000) 84:4693–6. doi:10.1103/PhysRevLett.84.4693
 25. Zhao Y, Tong L, Li Z, Yang N, Fu H, Wu L, et al. Stable and Multifunctional Dye-Modified Black Phosphorus Nanosheets for Near-Infrared Imaging-Guided Photothermal Therapy. *Chem Mater* (2017) 29:7131–9. doi:10.1021/acs.chemmater.7b01106
 26. Wang X, and Lan S. Optical Properties of Black Phosphorus. *Adv Opt Photon* (2016) 8:618–55. doi:10.1364/AOP.8.000618
 27. Xu Y, Wang Z, Guo Z, Huang H, Xiao Q, Zhang H, et al. Solvothermal Synthesis and Ultrafast Photonics of Black Phosphorus Quantum Dots. *Adv Opt Mater* (2016) 4:1223–9. doi:10.1002/adom.201600214
 28. Ghosh S, Winchester A, Muchharla B, Wasala M, Feng S, Elias AL, et al. Ultrafast Intrinsic Photoresponse and Direct Evidence of Sub-gap States in Liquid Phase Exfoliated MoS₂Thin Films. *Sci Rep* (2015) 5:11272. doi:10.1038/srep11272
 29. Tan SJR, Abdelwahab I, Chu L, Poh SM, Liu Y, Lu J, et al. Quasi-Monolayer Black Phosphorus with High Mobility and Air Stability. *Adv Mater* (2018) 30:1704619. doi:10.1002/adma.201704619
 30. Li X, Sun J, Shahi P, Gao M, MacDonald AH, Uwatoko Y, et al. Pressure-induced Phase Transitions and Superconductivity in a Black Phosphorus Single Crystal. *Proc Natl Acad Sci USA* (2018) 115:9935–40. doi:10.1073/pnas.1810726115
 31. Miao J, Song B, Li Q, Cai L, Zhang S, Hu W, et al. Photothermal Effect Induced Negative Photoconductivity and High Responsivity in Flexible Black Phosphorus Transistors. *ACS Nano* (2017) 11:6048–56. doi:10.1021/acsnano.7b01999

Conflict of Interest: The authors declare that the research was conducted in the absence of any commercial or financial relationships that could be construed as a potential conflict of interest.

Publisher's Note: All claims expressed in this article are solely those of the authors and do not necessarily represent those of their affiliated organizations, or those of the publisher, the editors and the reviewers. Any product that may be evaluated in this article, or claim that may be made by its manufacturer, is not guaranteed or endorsed by the publisher.

Copyright © 2021 Han, Jiang, Han, Dong and Gou. This is an open-access article distributed under the terms of the Creative Commons Attribution License (CC BY). The use, distribution or reproduction in other forums is permitted, provided the original author(s) and the copyright owner(s) are credited and that the original publication in this journal is cited, in accordance with accepted academic practice. No use, distribution or reproduction is permitted which does not comply with these terms.